Self-Channeling of High-Power Long-Wave Infrared Pulses in Atomic Gases

K. Schuh,* M. Kolesik, E. M. Wright, and J. V. Moloney
Department of Mathematics, Arizona Center for Mathematical Sciences, University of Arizona, Tucson, Arizona 85721, USA and College of Optical Sciences, University of Arizona, Tucson, Arizona 85721, USA

S. W. Koch
College of Optical Sciences, University of Arizona, Tucson, Arizona 85721, USA and Department of Physics and Material Science Center, Philipps-University, 35032 Marburg, Germany
(Received 28 October 2016; revised manuscript received 19 December 2016; published 10 February 2017)

We simulate and elucidate the self-channeling of high-power 10 μm infrared pulses in atomic gases. The major new result is that the peak intensity can remain remarkably stable over many Rayleigh ranges. This arises from the balance between the self-focusing, diffraction, and defocusing caused by the excitation induced dephasing due to many-body Coulomb effects that enhance the low-intensity plasma densities. This new paradigm removes the Rayleigh range limit for sources in the 8–12 μm atmospheric transmission window and enables transport of individual multi-TW pulses over multiple kilometer ranges.

DOI: 10.1103/PhysRevLett.118.063901

There are concerted efforts worldwide to develop sources of mid-wave (MWIR) and long-wave infrared (LWIR) high-power ultrashort laser pulses (USPs). These sources are intended to cover the important 3–5 [1–7] and 8–12 μm atmospheric transmission windows, and offer reduced scattering and mitigation against turbulence. Potential benefits of LWIR sources include longer stand-off distances for free-space optical communications applications, thermal imaging, remote detection of chemical agents, and enhanced propagation through fog and clouds. Applications of LWIR sources at long range are currently restricted by their Rayleigh range and the consequent requirement for large aperture beam launch conditions. By concentrating energy into USPs the hope is that the intrinsic nonlinearity of air constituents could balance diffraction effects and create high-intensity filaments at long range. Currently available MWIR 80 fs pulsed sources at 3.9 μm are limited to about 25 mJ in energy, around half the predicted required energy to sustain a high-power single filament over several tens of meter ranges [1]. In stark contrast, individual 800 nm filaments persist only over a meter range. USP sources in the 8–12 μm window with sufficient energy to potentially create a filament in air are currently limited to CO_2 gas lasers where recently 3 ps pulses with 45 J of energy (15 TW) have been reported [8].

A possible way forward in the quest for longer ranges is the recognition that the fundamental physics of USP propagation is altered at longer wavelengths. In particular, the well-known self-focusing collapse leading to extreme local intensities in the near infrared (NIR) [9] is no longer regularized via material dispersion plus free-electron plasma defocusing due to tunneling or multiphoton ionization. Instead, it is predicted that in the MWIR an optical carrier-wave shock develops before the collapse is established: This acts to limit the collapse by emitting recurrent bursts of dispersive waves that generate a broad featureless supercontinuum [1]. In this long wavelength scenario ionization through tunneling plays the relatively minor role of softening the extreme intensity spikes through additional weak plasma dispersion.

Looking to the LWIR region, further challenges to creating long-range filaments arise, including the growth of the critical power as λ^2, and the need to account for the quantum coherent nature of the light-matter interaction. Fortunately, recent advances in first-principles quantum calculations of the optical nonlinear response of gases [10] avoid the need for *ad hoc* phenomenological material modeling. This allows us to capture self-focusing, multiphoton, or tunneling ionization, as well as many-body effects within a single self-consistent theory. We stress that the many-body effects alluded to here occur between different atoms and not due to those in multielectron atoms [11,12]. Indeed we consider intensities that fall well below those for single-atom ionization. Here we demonstrate that the resulting many-body effects create a low density plasma, with associated plasma defocusing, that can lead to self-channeling in the LWIR. While it is negligible in the NIR, this defocusing contribution is relevant in the LWIR due to the high polarizability of free electrons at long wavelengths [10]. Specifically, we numerically demonstrate that the balance between the dynamic plasma defocusing, self-focusing, and diffraction can lead to a centimeter wide self-channeled 10 μm USP capable of sustaining high intensity over multiple Rayleigh ranges as evaluated for the incident beam, and can amount to kilometer ranges. We remark that filaments in the 3–4 μm infrared range and shorter are primarily sustained by an energy reservoir that tends to persist on the order of the Rayleigh range of the *initial* launch beam. In this context we note that previous claims to propagation over multiple

Rayleigh ranges at 800 nm have tended to use the narrower 100 μm filament diameter rather than refer to the launch beam diameter.

The many-body induced defocusing effect has been elaborated elsewhere [10] but here we describe it in terms that emphasize its relevance in the LWIR. For the far off-resonant conditions here, the light-matter interaction is in the regime of ultrafast adiabatic following for which the optical polarization is slaved to the instantaneous optical field $E(t)$. Likewise the occupation of the excited states follows the square of the exciting field, and the system returns to the ground state without any ionization after the excitation has passed. Dephasing in the form of multiphoton ionization, above threshold ionization, or tunnel ionization can break this adiabatic following leading to a net absorption. These are negligible in the present case, however, as we consider intensities well below those for single-atom ionization. An alternative dephasing mechanism is provided by many-body Coulomb interactions between atoms. In the field of optically excited semiconductors, it has been well established that the Coulomb scattering of the optically induced microscopic polarizations leads to dephasing. Since these processes depend on the degree of excitation in the system, these many-body effects are referred to as excitation-induced dephasing (EID). Detailed experiment-theory comparisons have shown that these EID effects can dominate light-matter coupling under suitable conditions [13].

Even though the effects of EID are well known in semiconductors, they have not previously been considered in atomic or molecular gases since these are so dilute compared to solid-state densities. However, Coulomb effects are strongly screened in solids, both by the background dielectric constant and by the dynamic screening of the optically induced material excitations. Background screening is pretty much absent in dilute gases and the density of optically induced excitations is rather low. Hence, the Coulomb interaction potential is only weakly screened and extremely long ranged, and it is not physically unreasonable that EID effects can become important for extreme nonlinear optics in gases.

In previous work we have shown that the EID mechanism enhances the ionization for intensities well below those for single-atom ionization, and leads to an increase in ionization that scales roughly with the square of the intensity [10]. EID leads to ionization degrees typically below 10^{-4} that have little impact on the propagation in the NIR or shorter wavelengths. However, it is known that the polarizability of free electrons increases as the square of the wavelength of the exciting field: This means that even low ionization degrees can have a significant impact on the nonlinear refractive index for the 8–12 μm LWIR wavelengths [10], where the polarizability of ionized electrons is 100–225 times larger than at 800 nm.

To focus on the many-body effects we concentrate on the example of argon: This avoids the complications of the nuclear motions associated with molecules while argon has similar electronic nonlinear properties to air. More specifically, for the many-body induced ionization we use the microscopic model presented in Ref. [10] and summarized in Sec. I of Supplemental Material [14]. The optical transitions are evaluated in the dipole approximation using a generalized version of the optical Bloch equations [13,21], which allow for the self-consistent analysis of the light-atom and the Coulombic many-body interactions [10]. Since it is not feasible to directly use such a numerically intensive microscopic model for the simulations of long-distance pulse propagation, we have developed a quantitative parametrization of the many-body results. In this way we capture the essential features of the microscopic quantum mechanical approach in a parametrized rate equation model for the plasma density $f(t)$. Since the dominant many-body contribution is the interaction between the transiently excited electrons, the ionization rate is proportional to the square of the electron excitation probability and thus $\propto E^4(t)$. We account for additional effects, such as weak dynamic screening and changing momentum distributions, using the phenomenological equation

$$\frac{d}{dt}f(t) = cE^4(t)\sqrt{\frac{E^2(t)+s}{E^2(t)}}, \tag{1}$$

with parameters c and s that are optimized by fitting to the full microscopic model; see Sec. II of Supplemental Material. Then free electrons that are accelerated by the pulsed electric field cause a defocusing contribution to the refractive index given by

$$n_{\mathrm{pl}} = -f(t)\frac{e^2\mu_0}{2m}\frac{\lambda^2}{(2\pi)^2}, \tag{2}$$

in addition to the usual Kerr self-focusing nonlinearity proportional to $E^2(t)$. The defocusing contribution increases quadratically with the wavelength λ, whereas the impact of the absorption associated with the generation of these free electrons is independent of the wavelength. Thus, plasma mediated defocusing is the dominant contribution caused by many-body effects in the LWIR.

As an illustration, Fig. 1 shows the computed ionization degree versus peak intensity for a 200 fs LWIR USP at 10 μm, the ionization degree being the ratio of the remnant plasma density after the USP has passed to the atomic density. The blue-dotted curve shows the ionization degree based on the single-atom ionization, and significant ionization appears only for intensities above 2×10^{17} W/m^2. The red curve shows the results from the full microscopic model, and the dashed black curve shows the results from the rate equation model plus the single-atom ionization. Thus, for intensities well below those for single-atom

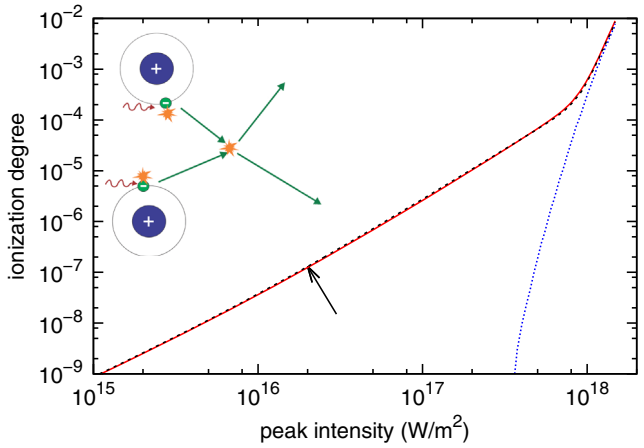

FIG. 1. Ionization degree versus peak intensity for a 200 fs LWIR USP at 10 μm. The blue-dotted curve shows the ionization degree based on single-atom ionization, the red curve shows the results from the full microscopic theory, and the dashed black curve shows the results from the rate equation model supplemented by the single-atom ionization. Here the optimized fit parameters $c = 3.04 \times 10^{-7}$ $(1/\mathrm{m^3 s})$ $(\mathrm{m^4/V^4})$ and $s = 4.6 \times 10^{18}$ $(\mathrm{V^2/m^2})$ were employed for argon at 1 atm. The arrow indicates the peak intensity reached in our propagation simulations, and this remains well below the threshold value 2×10^{17} $\mathrm{W/m^2}$ for single-atom ionization. The inset illustrates that the many-body interaction involves electrons from different atoms.

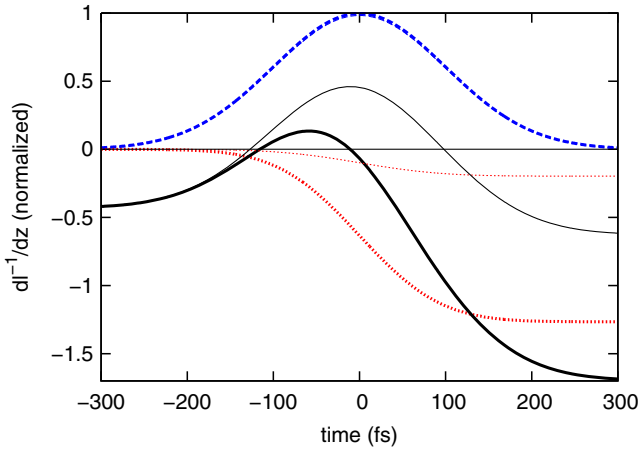

FIG. 2. Kerr lensing (blue-dashed curve) and dynamic plasma lensing (red-dotted curves) contributions as functions of time delay with respect to the pulse center; see Sec. III of Supplemental Material. The black curves show the net lensing experienced by the pulse including diffraction. Results are for a 10 (wide lines) and 4 μm (thin lines, parameters in brackets if different) USP of beam width 1.2 (0.48) cm, length 240 fs, peak intensity 1.5×10^{16} $\mathrm{W/m^2}$, corresponding to a peak power of 2.4 (0.38) TW equivalent to 1.6 critical powers, and a pulse energy of 590 (94) mJ. The values are scaled to the maximum of the Kerr contribution for each pulse, respectively.

ionization, the full microscopic model and phenomenological rate equation agree very well and display enhanced ionization due to EID.

In the remainder of this Letter we elucidate our case that EID induced defocusing can balance Kerr self-focusing to produce self-channeling of USPs that can extend over kilometer ranges. Our simulations use the fully optical carrier wave resolved unidirectional pulse propagation model [22], which can incorporate any given user-supplied nonlinear optical response. Here, we are including both the single-particle, i.e., isolated atom, and the many-body source terms to describe the polarization response. Thus, we combine the many-body ionization rate in Eq. (1) with an ionization term fitted to the single-particle strong-field ionization to describe the total ionization rate. The resulting polarization response of the ionized electrons including the many-body effects is complemented with a Kerr nonlinearity using $n_2 = 9.8 \times 10^{-24}$ $\mathrm{m^2\,W^{-1}}$ based on Ref. [23]. This value accounts for the weak dependence on wavelength in the MWIR and LWIR caused by the off-resonant electronic transitions. See Sec. II A of Supplemental Material for details.

To frame our simulations, Fig. 2 depicts the competing nonlinear lensing contributions for a 4 μm MWIR (thin lines) and a 10 μm LWIR (wide lines) USP of 240 fs duration (see the figure caption for other parameters). As described in Sec. III of Supplemental Material, the lensing from the self-focusing and plasma defocusing effects is calculated as the rate of change with propagation distance z of the inverse focal length $l(z,t)$. More specifically Fig. 2 shows the contributions of Kerr lensing (blue-dashed curve) and dynamic plasma lensing (red-dotted curves) as functions of time delay with respect to the pulse center. The Kerr lensing tracks the modulus squared of the pulsed electric field envelope as expected for the instantaneous Kerr effect, whereas the many-body contribution yields a time-integrated negative response, as expected from Eq. (2). The black curves in Fig. 2 show the net lensing experienced by the USPs including diffraction. We see that the many-body mediated lensing can indeed balance the nonlinear Kerr focusing of the LWIR USP to a large extent prohibiting strong focusing and thereby allowing for self-channeling. In contrast, the many-body effects cause only a minor change in the nonlinear focusing of the MWIR USP. In Sec. III of the Supplemental Material we further discuss the intensity, wavelength, and pulse length dependence of the anticipated self-channeling. Here we point to the important trend that for MWIR and shorter wavelengths the many-body lensing is reduced with respect to the Kerr lensing by virtue of Eq. (2), and the self-channeling balance is less tenable. Likewise, for longer LWIR wavelengths, the combination of stronger many-body negative lensing and increased diffraction makes any kind of self-focusing more problematic. Thus, the window of opportunity for many-body mediated self-channeling is in the LWIR around 10 μm.

Figure 3 shows the peak intensity versus propagation distance for both 4 μm MWIR and 10 μm LWIR USPs over a distance of 130 m. We contrast the situation where the

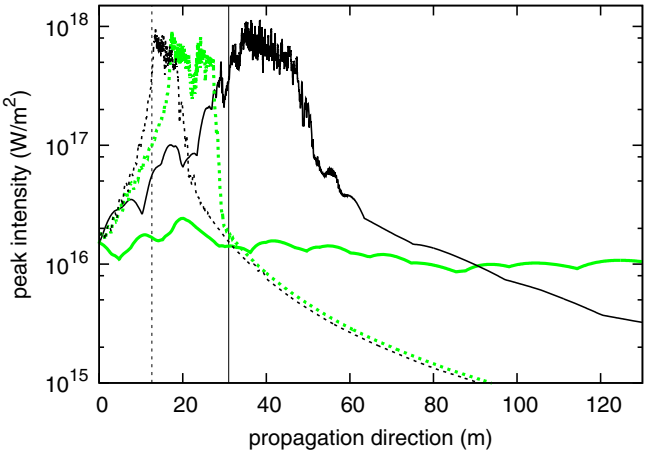

FIG. 3. Peak intensity versus propagation distance for 4 μm MWIR (dashed curves) and 10 μm LWIR (solid curves) USPs. The results based on the single-atom model are the black curves, and those based on the many-body model are the green or gray curves. The Rayleigh range of the MWIR beam is 16 m (vertical dashed line) and that of the LWIR is 31 m (vertical line). The solid green or gray line shows the many-body mediated self-channeling.

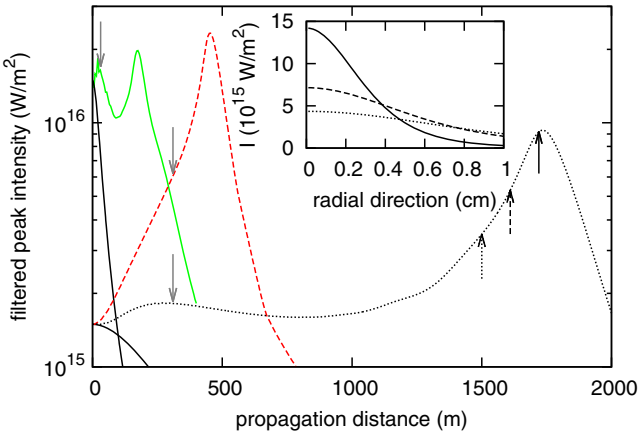

FIG. 4. Spectrally filtered peak intensity versus propagation distance for different 10 μm LWIR USPs. The green curve is for a 2.4 TW USP of 240 fs duration and 1.2 cm wide (same as in Fig. 3), the red-dashed curve is for 240 fs and 3.7 cm, and the black-dotted curve is for 1.2 ps and 3.7 cm. The gray arrows indicate the Rayleigh ranges of 31 and 310 m, respectively, while the black solid curves indicate the intensities for linearly propagating beams. The inset shows the unfiltered radial intensity of the 1.2 ps USP at the positions indicated by the black arrows with matching line style. The initially 3.7 cm wide pulse collapses down to 0.6 cm.

nonlinear optical response is computed from a single-atom model corresponding to the blue-dotted ionization curve in Fig. 1 and our many-body model (red curve). The USP parameters used to generate this figure are identical to those used for Fig. 2. For the MWIR USP (dashed curves) the many-body influences (green or gray dashed curve) are relatively minor as shown in Fig. 2 and just shift the extremum of the peak intensity a few meters downstream relative to the single-atom model (black-dashed curve) while retaining the same initial sharp self-focusing onset. Here many-body mediated effects only mildly oppose the dominant self-focusing lensing action. The contrast between the LWIR (solid curves) single-atom and many-body model propagation results is, however, dramatic as suggested by the strong contribution to negative lensing at 10 μm in Fig. 2: While the single-atom model (black curve) still retains the characteristics of beam collapse due to self-focusing, the many-body result (green or gray curve) displays a remarkably constant peak intensity over the full propagation distance, indicative of self-channeling of the LWIR USP. Figure 3 therefore shows self-channeled propagation over multiple Rayleigh ranges, the Rayleigh range being 31 m as indicated by the vertical solid line. In fact, the self-channeled beam propagates even further but at the expense of generating broad higher harmonic components; see Sec. IV of Supplemental Material for more details.

Finally, we test whether collimated self-channeled 10 μm USPs can be launched and sustained over even longer kilometer ranges. To this end we scale up the beam waist to 3.7 cm, which yields a Rayleigh range of 310 m. The peak power is kept at 2.4 TW to maintain it at 1.6 critical powers as in Fig. 3. Figure 4 shows many-body model simulations for a 240 fs USP with 1.2 cm waist (green curve) as in Fig. 3, a 240 fs USP with 3.7 cm waist (red-dashed curve) and 590 mJ pulse energy, and finally a 1.2 ps USP with the same properties but 3 J pulse energy (black-dotted curve). In contrast to the data shown in Fig. 3, we apply a band-pass filter function at the end of the propagation that spans a broad bandwidth about the fundamental to block out higher harmonics. The reason for this is the appearance of higher harmonic features downstream in the propagation that can cause transient intensities that can exceed and obscure that of the fundamental pulse while constituting only a small part of the pulse energy. We display and discuss these features in Sec. IV of Supplemental Material. The results shown in Fig. 4 indicate that it is indeed possible to launch a self-channeled USP well beyond a kilometer if the launch conditions avoid strong initial focusing. The key difference between the 240 fs and 1.2 ps cases lies in the fact that the longer pulse accumulates stronger ionization, which strengthens the negative dynamic lensing relative to the instantaneous Kerr effect. The softer positive lens avoids an initial strong-field focusing, which dynamically shuts off the positive lens and rapidly defocuses the beam as shown by the shorter 240 fs USP (red-dashed curve). We still observe a relatively strong focusing around 1.5 km with a subsequent shut off of the positive lens and defocusing around 2 km. This focusing is caused by an effective shortening of the USP as illustrated in Figs. 8 and 9 of Supplemental Material. While this pulse shortening has no impact on the instantaneous Kerr focusing it leads to a

reduction of the many-body induced plasma defocusing and disrupts the balance underpinning the self-channeling. The focusing is regularized by the dispersive walk-off of higher frequency components [1] leading to a subsequent defocusing.

In summary, we have presented a comprehensive study of the influence of many-body induced dephasing effects on the nonlinear propagation of intense ultrashort laser pulses at 10 μm wavelength. For these LWIR USPs the rather low ionization significantly changes the propagation due to the larger polarizability of the liberated electrons. Although the intrinsic diffraction, many-body induced dephasing effects, and nonlinearity are all very weak, we observe how all three act in concert to create a significant macroscopic modification of the pulse propagation characteristics. In particular, the increased ionization due to many-body effects contributes to a regularization of the Kerr induced focusing and thus is able to stabilize the peak intensity and create, for the first time, genuine self-channeling of USPs over multiple Rayleigh ranges. We close by remarking that self-channeling was initially proposed as the mechanism of filament formation in the near infrared, but there absorption associated with plasma generated via multiphoton ionization disallowed long-range propagation [24]. It is satisfying that many-body Coulomb interactions, often considered irrelevant in atomic gases, have made the self-channeling scenario viable in the long-wave infrared.

This material is based upon work supported by the Air Force Office of Scientific Research under Grants No. FA9550-16-1-0088 and No. FA9550-15-1-0272.

*kschuh@optics.arizona.edu

[1] P. Panagiotopoulos, P. Whalen, M. Kolesik, and J. V. Moloney, Nat. Photonics **9**, 543 (2015).
[2] A. V. Mitrofanov, A. A. Voronin, D. A. Sidorov-Biryukov, A. Pugžlys, E. A. Stepanov, G. Andriukaitis, T. Flöry, S. Ališauskas, A. B. Fedotov, A. Baltuška, and A. M. Zheltikov, Sci. Rep. **5**, 8368 (2015).
[3] B. Shim, S. E. Schrauth, and A. L. Gaeta, Opt. Express **19**, 9118 (2011).
[4] M. Cheng, A. Reynolds, H. Widgren, and M. Khalil, Opt. Lett. **37**, 1787 (2012).
[5] Y. Nomura, H. Shirai, K. Ishii, N. Tsurumachi, A. A. Voronin, A. M. Zheltikov, and T. Fuji, Opt. Express **20**, 24741 (2012).
[6] D. Kartashov, S. Ališauskas, A. Pugžlys, A. Voronin, A. Zheltikov, M. Petrarca, P. Béjot, J. Kasparian, J.-P. Wolf, and A. Baltuška, Opt. Lett. **38**, 3194 (2013).
[7] L. Bergé, J. Rolle, and C. Köhler, Phys. Rev. A **88**, 023816 (2013).
[8] D. Haberberger, S. Tochitsky, and C. Joshi, Opt. Express **18**, 17865 (2010).
[9] A. Couairon and A. Mysyrowicz, Phys. Rep. **441**, 47 (2007).
[10] K. Schuh, J. V. Moloney, and S. W. Koch, Phys. Rev. E **93**, 013208 (2016).
[11] A. Becker, L. Plaja, P. Moreno, M. Nurhuda, and F. H. M. Faisal, Phys. Rev. A **64**, 023408 (2001).
[12] A. Becker and F. H. M. Faisal, J. Phys. B **38**, R1 (2005).
[13] H. Haug and S. W. Koch, *Quantum Theory of the Optical and Electronic Properties of Semiconductors* (World Scientific Publishing Company, Singapore, 2004).
[14] See Supplemental Material http://link.aps.org/supplemental/10.1103/PhysRevLett.118.063901 for additional informations about the used models and a discussion of the results in more detail, which includes Refs. [15–20].
[15] K. Schuh, J. Hader, J. V. Moloney, and S. W. Koch, Phys. Rev. E **89**, 033103 (2014).
[16] K. Schuh, J. Hader, J. V. Moloney, and S. W. Koch, J. Opt. Soc. Am. B **32**, 1442 (2015).
[17] H. Haug and A.-P. Jauho, *Quantum Kinetics in Transport and Optics of Semiconductors*, 2nd ed. (Springer-Verlag, Berlin, 2008).
[18] P. Lipavský, V. Špička, and B. Velický, Phys. Rev. B **34**, 6933 (1986).
[19] M. Kolesik and J. V. Moloney, Phys. Rev. E **70**, 036604 (2004).
[20] E. M. Wright, B. L. Lawrence, W. Torruellas, and G. Stegeman, Opt. Lett. **20**, 2481 (1995).
[21] W. Schäfer and M. Wegener, *Semiconductor Optics and Transport Phenomena* (Springer, New York, 2002).
[22] M. Kolesik and J. V. Moloney, Phys. Rev. E **70**, 036604 (2004).
[23] S. Zahedpour, J. K. Wahlstrand, and H. M. Milchberg, Opt. Lett. **40**, 5794 (2015).
[24] M. Mlejnek, E. M. Wright, and J. V. Moloney, IEEE J. Quantum Electron. **35**, 1771 (1999).